J. Fluid Mech. (2001), *vol.* 442, *pp.* 335–358. Printed in the United Kingdom

On an instability to Langmuir circulations and the role of Prandtl and Richardson numbers

By W. R. C. PHILLIPS

Department of Theoretical and Applied Mechanics,
University of Illinois at Urbana-Champaign, Urbana, IL 61801-2935, USA.

(Received 20 September 2000 and in revised form 5 March 2001)

The instability of a weakly sheared density-stratified two-dimensional wavy flow to longitudinal vortices is considered. The instability mechanism is Craik–Leibovich type 2, or CL2, and the problem is posited in the context of Langmuir circulations beneath irrotational wind-driven surface waves. Of interest is the influence to the instability of Prandtl Pr and Richardson Ri numbers according to linear theory. The basis for the study is an initial value problem posed by Leibovich & Paolucci (1981) in which the liquid substrate is of semi-infinite extent and the wind-driven current is permitted to grow in the presence of neutral waves. In the present work Pr is varied from zero to infinity, and both stabilizing and destabilizing Ri are considered; so too are monochromatic and measured wave fields, and laminar and turbulent velocity profiles. Only the $Ri = 0$ results recover those of Leibovich & Paolucci. For stabilizing Ri, it is found in general that diminishing Pr are destabilizing to Langmuir circulations (LCs), and thus that LCs can be present or absent at the same Langmuir number La provided $Ri \neq 0$. It is further found that two branches of neutral curves occur for some combinations of Pr and Ri, and that minor changes in either parameter permit the preferred spacing to switch from one branch to the other. In consequence the preferred spanwise spacing may change from smaller than the wavelength of the dominant waves to larger than it. Furthermore, although LCs will not form at inverse La below a global lower bound given by an energy stability analysis, the actual value of La at onset is found to depend greatly upon local details of the wave and shear fields. Interestingly although this global lower bound is independent of Ri and Pr for $Ri \geqslant 0$, that is not the case for $Ri < 0$, where it approaches zero as $Ri \to -\infty$, indicating that the CL2 instability is viable even at low Reynolds numbers.

1. Introduction

This paper is concerned with the role Prandtl and Richardson numbers play in the formation of organized convective motions known as Langmuir circulations, or LCs, which form in the surface layer of oceans, lakes and ponds when winds of moderate strength blow over them. LCs act at the surface to concentrate flotsam, seaweed, oil and/or air bubbles into clearly visible streaks or bands known as windrows, with spacings ranging from a few millimetres (Kenney 1993) to several hundred metres (Plueddemann *et al.* 1996). This feature has captured the attention of mariners and scientists for eons, but it was Langmuir (1938) who realized that windrows are visible manifestations of a parallel series of counter-rotating vortices in the surface layer of the water beneath that more or less align with the wind.

Langmuir's observations further led him to believe that the vortices are largely

responsible for the formation of thermoclines and the maintenance of mixed layers in lakes and oceans. This notion is compelling, in part because of the importance of the mixed layer and the heat, mass and momentum transport processes therein (see e.g. Li, Zahariev & Garrett 1995), but also because LCs are apparently orderly flow structures that arise out of disorderly environments. In consequence many attempts have been made to explain them, but of the range of models suggested (see reviews by Leibovich 1983 and Gargett 1989), the most plausible have as their basis a nonlinear interaction between surface gravity waves and a weak current.

Of interest here is the prevailing theory in this category, that of Craik & Leibovich (1976) (see also Craik 1970 and Leibovich & Ulrich 1972). These authors provide a rational derivation of a set of equations – the CL-equations – thought to govern LCs, given an irrotational wave field in which the wave slope is $O(\epsilon)$ and an $O(\epsilon^2)$ wind-driven rotational mean current. The CL-equations also follow from Andrews & McIntyre's (1978) exact theory of nonlinear waves on a Lagrangian-mean flow (Leibovich 1980), in which the nonlinear interaction of the waves with themselves is represented as a rectified $O(\epsilon^2)$ effect through the Stokes drift. Interestingly, the CL-equations predict that activity akin to Langmuir circulations may result from either of two instability mechanisms, CL1 or CL2.

CL1 requires a surface wave field with a high degree of spatial structure while CL2 acts without special spatial structure (Craik 1977; Leibovich 1977*a*). However because spatial variations in the Stokes drift diminish owing to phase mixing as the number of components in the wave spectrum increases (Craik & Leibovich 1976), CL2 is thought the most relevant in the ocean context. In consequence CL2 has formed the basis for numerous studies concerned with LCs and the effect on them of stratification, nonlinearity and streamwise growth (e.g. Leibovich & Paolucci 1980, 1981; Leibovich, Lele & Moroz 1989; Cox *et al.* 1992; Cox & Leibovich 1993, 1997; Li & Garrett 1993, 1997; Skyllingstad & Denbo 1995; McWilliams, Sullivan & Moeng 1997).

Further details of ocean LCs have also emerged from a vast observational program (Thorpe & Hall 1982; Weller *et al.* 1985; Smith, Pinkel & Weller 1987; Weller & Price 1988; Zendel & Farmer 1991; Smith 1992, 1998; Plueddemann *et al.* 1996 and others). But comparison with CL-theory neither convincingly endorses nor convincingly refutes CL2. For example Smith (1992) details an occurrence in the Pacific ocean in which LCs are absent in the presence of essentially steady waves and wind in a breeze of $8\,\mathrm{m\,s^{-1}}$, but form within fifteen minutes of the wind freshening to $13\,\mathrm{m\,s^{-1}}$. When first observed, the windrow spacing (i.e. spanwise wavelength of the LCs) was about two thirds the wavelength of the dominant waves, but grew over the next hour to about twice the dominant wavelength. What is striking about these findings, *vis à vis* CL2, is that they indicate the absence and presence of LCs at essentially the same Langmuir number La, the key parameter in CL-theory (La is defined in § 2). Furthermore the initial windrow spacings are a factor of five or so smaller than predicted, at least at zero Richardson number. But Smith's lament in comparing his observations with CL2 is not the instability *per se*, but rather the absence of more detailed parametric studies of the first bifurcation to LCs via CL2, specifically the role of Prandtl number Pr, Richardson number Ri and the influence of growing waves.

Our intent here is to focus upon the effects of Pr and Ri (the role of growing waves is considered elsewhere, Phillips 2001*b*) and do so via an initial value problem posed by Leibovich & Paolucci (1981, henceforth LP), outlined in § 2. In essence they take the view that the instability works its way down from the surface, following the

imposition there of a wave field and a wind stress; the layer may then be thought of as infinitely deep and the shear within it to resemble a Rayleigh stress layer. LP considered one value of Pr and three values of Ri, which we recalculate in § 3: interestingly, while we concur with their $Ri = 0$ results, we conclude that their $Ri > 0$ results are flawed. We go on to consider a wide range of Pr at stabilizing Ri in § 4 and destabilizing Ri in § 5. In doing so we find that diminishing Prandtl numbers at non-zero Richardson numbers are destabilizing to LCs. We further find that small changes to some combinations of Pr and Ri permit the preferred spacing to jump from smaller than the wavelength of the dominant waves to larger than it, in accord with Smith's observations (§ 4.4). A feature also of interest is the influence on onset of the input profiles of mean velocity and Stokes drift. We explore this in § 6 using Stokes drift profiles based upon Smith's (1992) ocean measurements and mean velocity profiles akin to those in a bounded turbulent boundary layer. We determine that La at onset is strongly influenced by Ri, Pr and local details of the shear and wave spectrum. Our results are discussed in § 7.

2. Governing equations

2.1. *Background*

We consider the formation of LCs beneath surface waves of characteristic slope $\epsilon \ll 1$ in the presence of wind-driven shear in deep water, via an initial value problem posed by LP. Here the water is initially at rest and its temperature varies as $T(z)$. At time $t = 0$ a wind stress and surface waves are imposed. The wind stress is represented by the interface friction velocity u_* in the wind direction and causes the velocity in the water to grow, while the wave field is assumed to be neutral and to also propagate in the wind direction, which we take to be the x-direction. Further, we let the mean free surface coincide with the (x, y)-plane and set z positive vertically upwards.

Key parameters are thus u_*, wave frequency σ, streamwise wavenumber α and amplitude a, which together define a characteristic velocity scale $\mathscr{V}$ and thus the level of shear in the water through $\mathscr{V}\alpha/\sigma = O(\epsilon^s)$ where $s \geqslant 0$ (see Phillips 1998). Of course $s \in [0, 2]$ at any instant in the open ocean (Melville, Shear & Veron 1998), but the phase velocity of dominant waves is typically $O(\epsilon^{-2})$ larger than $\mathscr{V}$, so that $s = 2$, and that is the case we consider.

The waves are then irrotational and interact with themselves (nonlinearly) to yield a mean drift velocity, the Stokes drift, with one non-zero component $\alpha\sigma a^2 D_1$ in the direction of wave propagation. Furthermore, the ensuing $O(\epsilon)$-wave $O(\epsilon^2)$-mean flow interaction is described by the CL-equations (Craik & Leibovich 1976) and can be unstable to LCs via the CL1 mechanism if $D_1 = D_1(y, z)$, or CL2 if $D_1 = D_1(z)$ (Craik 1977; Leibovich 1983). In the ocean context, however, where the waves comprise a continuous spectrum of wavenumbers of random phase, it follows that Fourier components in the spanwise y-direction phase mix to zero (Craik & Leibovich 1976), so that CL2 (or more precisely CL2-$O(\epsilon^2)$, Phillips, Wu & Lumley 1996) is relevant, and that is the instability mechanism considered here.

The CL-equations may be non-dimensionalized in various ways but we follow Leibovich (1977*a*). In particular we introduce spatial and temporal scales as

$$\left[(x, y, z)\alpha^{-1},\ \frac{t}{a\alpha u_*}\left(\frac{\nu_T}{\sigma}\right)^{1/2}\right], \tag{2.1}$$

with, because $\mathscr{V} = u_*^2/\alpha\nu_T$, corresponding mean and perturbation velocity components

$$\left[(U(z,t)+u(y,z,t))\mathscr{V},(v(y,z,t),w(y,z,t))u_*a\left(\frac{\sigma}{\nu_T}\right)^{1/2}\right]. \tag{2.2}$$

Accordingly the temperature perturbation is $\vartheta T'/\alpha$, where prime denotes $\mathrm{d}/\mathrm{d}z$ and ν_T is an eddy viscosity representative of turbulent diffusivity of momentum. Finally, with streamwise-averaged (dimensionless) Eulerian velocity perturbations $\boldsymbol{u} = (u, v, w)$, unit vectors $(\boldsymbol{i}, \boldsymbol{j}, \boldsymbol{k})$ in (x, y, z) respectively and $\mathrm{D} \equiv \partial/\partial z$, the ensuing perturbation equations relative to the substrate $U(z,t)$ and linear thermocline $T(z)$ are (LP)

$$\frac{\partial \boldsymbol{u}}{\partial t} + \boldsymbol{u}\cdot\nabla\boldsymbol{u} = D_1\nabla u - w\mathrm{D}U\boldsymbol{i} + Ri\vartheta\boldsymbol{k} - \nabla p + La\nabla^2\boldsymbol{u} \tag{2.3a}$$

and

$$\frac{\partial \vartheta}{\partial t} + \boldsymbol{u}\cdot\nabla\vartheta = -w + LaPr^{-1}\nabla^2\vartheta \quad \text{with} \quad \nabla\cdot\boldsymbol{u} = 0. \tag{2.3b}$$

Here La is the Langmuir number

$$La = \frac{\alpha\nu_T}{au_*}\left(\frac{\nu_T}{\sigma}\right)^{1/2}, \tag{2.4}$$

Pr is a turbulent Prandtl-number (where κ_T is the eddy diffusivity of heat)

$$Pr = \frac{\nu_T}{\kappa_T}$$

and Ri is a Richardson number

$$Ri = \frac{N^2}{(au_*\alpha)^2(\sigma/\nu_T)},$$

where $N^2 = \beta g T'(z)$ is the Brunt–Väisälä frequency with β the thermal coefficient of expansion and g gravity. Also useful is the gradient Richardson number Ri^*, based upon N^2 and the geometric mean of U' and D_1' (Smith 1992); Ri^* and Ri are, of course, related (see § 3.1).

The initial value problem is completed with the boundary conditions

$$\boldsymbol{k}\cdot\boldsymbol{u} = \mathrm{D}(\boldsymbol{u}\times\boldsymbol{k}) = \vartheta = 0 \quad \text{on} \quad z = 0, \tag{2.5a}$$

$$\boldsymbol{u} \to 0, \quad \vartheta \to 0 \quad \text{as} \quad z \to -\infty, \tag{2.5b}$$

the initial values

$$\boldsymbol{u}(\boldsymbol{x},0) = \boldsymbol{u}_0(\boldsymbol{x}), \vartheta(\boldsymbol{x},0) = 0, \tag{2.5c}$$

and the requirement that $\boldsymbol{u}_0(\boldsymbol{x})$ is solenoidal.

2.2. *Numerical formulation*

Our intent is to proceed numerically, but prior to doing so it is prudent to rewrite (2.3). In particular we seek a form that assumes the LCs are spanwise periodic with wavenumber l and, because the substrate is a boundary layer, ensures that the perturbations approach a constant value exponentially fast as $z \to -\infty$ (see below). In consequence we write

$$(\boldsymbol{u}, p, \vartheta) = [\hat{\boldsymbol{u}}(z,t), \hat{p}(z,t), \hat{\vartheta}(z,t)]\mathrm{Re}\{\mathrm{e}^{\gamma z + \mathrm{i}ly}\} \tag{2.6}$$

where $\gamma \geqslant 0$ is a constant. Finally we map from the semi-infinite plane to the finite plane with the transformation $\zeta = \mathrm{e}^z$, rendering $\mathrm{D} \equiv \zeta\partial/\partial\zeta$.

On cross-differentiating to eliminate $\hat{p}$, we then have

$$\frac{\partial \hat{u}}{\partial t} = -\hat{w}\mathrm{D}U + La(\mathrm{M} - l^2)\hat{u}, \tag{2.7a}$$

$$(\mathrm{M} - l^2)\frac{\partial \hat{w}}{\partial t} = l^2\hat{u}\mathrm{D}D_1 + La(\mathrm{M} - l^2)^2\hat{w} - l^2 Ri\hat{\vartheta} \tag{2.7b}$$

and

$$\frac{\partial \hat{\vartheta}}{\partial t} = -\hat{w} + LaPr^{-1}(\mathrm{M} - l^2)\hat{\vartheta} \tag{2.7c}$$

in accord with LP, but with the general operator

$$\mathrm{M} \equiv \zeta\frac{\partial}{\partial\zeta}\left(\zeta\frac{\partial}{\partial\zeta}\right) + 2\gamma\zeta\frac{\partial}{\partial\zeta} + \gamma^2$$

and boundary conditions

$$\frac{\partial \hat{u}}{\partial\zeta} + \gamma\hat{u} = \hat{w} = \frac{\partial^2\hat{w}}{\partial\zeta^2} + (1 + 2\gamma)\frac{\partial\hat{w}}{\partial\zeta} + \gamma^2 = \hat{\vartheta} = 0 \quad \text{on} \quad \zeta = 1, \tag{2.8a}$$

and

$$\hat{u} = \hat{w} = \hat{\vartheta} = 0 \quad \text{with all derivatives bounded on} \quad \zeta = 0. \tag{2.8b}$$

Equations (2.7) with (2.8) and $\gamma = 0$ were solved numerically by LP using Galerkin techniques which they outline in detail. Briefly the dependent variables $\hat{u}$, $\hat{w}$ and $\hat{\vartheta}$ are each expanded in linearly independent, complete sets of basis functions truncated after N terms. The time-dependent coefficients multiplying the basis functions at each order, $\boldsymbol{a}(t)$ say, are unknown. Substitution into (2.7) and evaluation of the inner products then leads to a system of $3N$ linear, homogeneous algebraic equations of the form

$$\frac{\mathrm{d}\boldsymbol{a}}{\mathrm{d}t} = \boldsymbol{A}(t)\boldsymbol{a} \tag{2.9}$$

where the elements of the matrix $\boldsymbol{A}(t)$ are known from the inner products.

Since the numerical technique carries over to the $\gamma \neq 0$ case we follow suit but with various numerical improvements: First, in order to satisfy the physical requirement in unbounded laminar (see Brown & Stewartson 1965; Phillips 1996) and turbulent flows (Phillips & Ratnanather 1990) that the velocity field approach a constant value exponentially fast as $z \to -\infty$, we set $\gamma = 1$. Failure to satisfy this requirement can cause convergence problems owing to spurious singular behaviour arising from truncation of the basis functions at finite N (Spalart, Moser & Rogers 1991). Furthermore, requiring $\gamma = 1$ has the advantage of rendering the results insensitive to the choice of boundary conditions at large z, because (2.6) demands both $\boldsymbol{u}$ and $\partial\boldsymbol{u}/\partial z$ be homogeneous as $z \to \infty$. Second, rather than use *ad hoc* polynomials for the basis functions as LP did, we employ Chebyshev polynomials, whose properties can be exploited by Gaussian quadrature, which we use for accurate, efficient integration of the inner products. Finally the eigenvalue problem (2.9) was solved using LaPak with $N = 25$.

Of course (2.6) may be recast to describe other linear stability problems, albeit with different operators and boundary conditions, and these provided useful test cases to validate our computer code. Examples employed included the Dean problem, which utilizes (2.7*a*) and (2.7*b*) (see Drazin & Reid 1981), and the thermohaline Rayleigh–Jeffreys problem (Baines & Gill 1969; Leibovich *et al.* 1989) which incorporates all

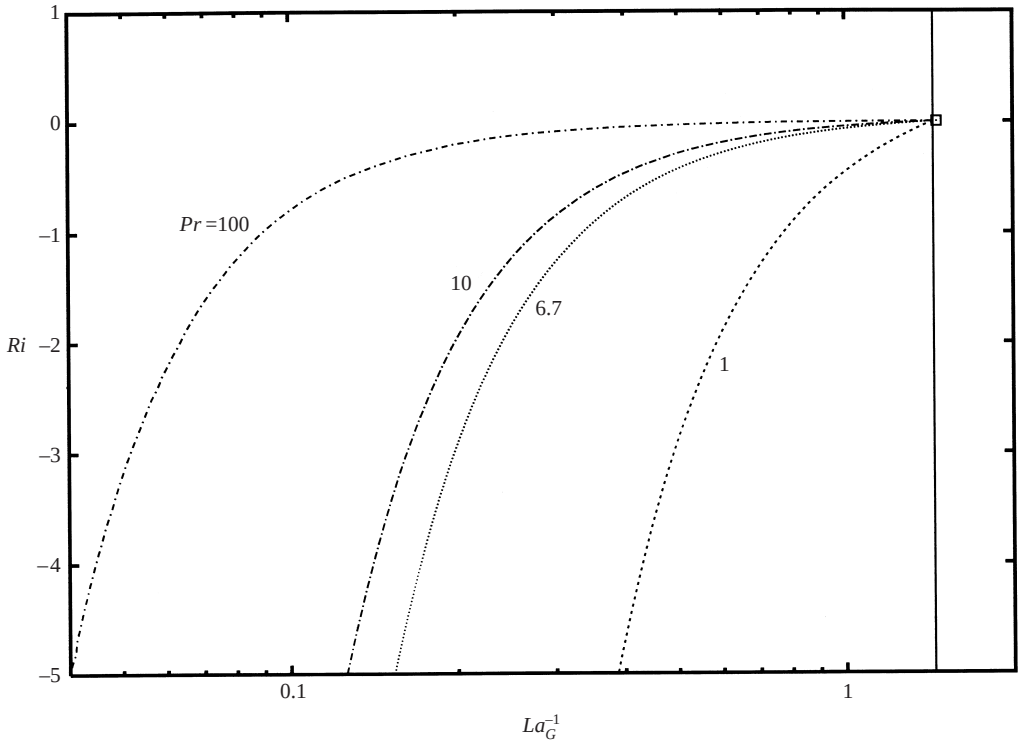

FIGURE 1. Curves showing Richardson number against the optimal global stability limit La_G^{-1} for various Prandtl numbers in the $t \to \infty$ limit. Note that La_G^{-1} is independent of Ri and Pr for stabilizing, i.e. positive Ri, indicated by vertical line. Symbol □ denotes Leibovich & Paolucci's (1981) $Ri = 0$ result from table 1.

components of (2.7). In each instance we accurately recovered the published onset values, and in the case of Leibovich *et al.*, the whole of their figure 1.

3. Leibovich & Paolucci revisited

3.1. *Base flow*

For the purpose of comparison we begin by revisiting the problem investigated by LP. Here the developing substrate velocity $U(z,t)$ is given by a solution to the stress Rayleigh problem as

$$U = 2\left(\frac{tLa}{\pi}\right)^{1/2}[\exp(-\eta^2) - \pi^{1/2}\eta\,\mathrm{erfc}(\eta)], \tag{3.1a}$$

where

$$\eta = -\frac{z}{2(tLa)^{1/2}}$$

so that

$$\mathrm{D}U = \mathrm{erfc}(\eta). \tag{3.1b}$$

Accordingly the Stokes drift for monochromatic irrotational neutral waves is taken to be

$$D_1 = 2\mathrm{e}^{2z} \quad (-\infty < z \leqslant 0), \tag{3.2}$$

from which it follows that $Ri = 4Ri^*$.

Ri	La_G^{-1}	l_G	σ_1	σ_2	La_c^{-1}	l_c	V_c	$La_G^{-1}\|_{LP}$	$l_G\|_{LP}$	$La_c^{-1}\|_{LP}$	$l_c\|_{LP}$
0	1.4395	0.3331	0.2631	1.000	1.5157	0.3187	0	1.46	0.32	1.52	0.32
0.1					2.6896	0.3469	$\pm$0.0416				
0.1					3.7281	0.2415	0			1.58	0.31
0.25					5.6517	0.6767	$\pm$0.0893				
0.25					6.5868	0.2477	0			1.66	0.30

TABLE 1. Global and critical inverse Langmuir numbers La_G^{-1}, La_c^{-1} and critical wavenumbers l_G, l_c of linear theory at various Richardson numbers with $Pr = 6.7$, compared with those of Leibovich & Paolucci (1981). Note that dual values at $Ri > 0$ depict critical values on the upper and lower branches of the neutral curve; solutions on the upper branch are convective while those on the lower branch are stationary.

3.2. *Global stability*

LP confined attention to one Prandtl number, $Pr = 6.7$, and deduced regions of stability for three Richardson numbers, $Ri = 0$, 0.1 and 0.25; they began their study with an energy stability analysis. This sought to isolate a global lower bound for La^{-1} via a set of equations not dissimilar to the steady-state form of (2.7) but which, in addition to Ri and Pr, depend parametrically on two further variables, σ_1 and σ_2. The lower bound, La_G^{-1} say, is found by first minimizing La^{-1} over all $t \geqslant 0$ and $l \geqslant 0$ and then maximizing this minimum over all admissible values of σ_1 and σ_2. Specifically, because $Pr \geqslant 0$, the analysis requires both σ_1 and $\sigma_2 Ri$ be non-negative for all Ri. If a finite La_G^{-1} exists, then global monotonic stability is assured if $La^{-1} < La_G^{-1}$. LP restricted attention to stabilizing or neutral Richardson numbers, i.e. $Ri \geqslant 0$ and report $(La_G^{-1}, l_G) = (1.46, 0.32)$ for $Ri = 0$ with other values for $Ri > 0$; but Leibovich (1983) later noted that La_G^{-1} is independent of Ri in stably stratified conditions.

Using the numerical techniques of § 2.2 to solve the energy stability equations (LP's equation (20) subject to (2.6)), we computed La_G^{-1} for a wide range of $Ri \gtrless 0$ and $Pr \geqslant 0$ and traces of La_G^{-1} in the range $Ri \in [-5, 1]$ for various Prandtl numbers are shown in figure 1. First, we concur with LP's result that the least-stable wave–mean interaction occurs in the $t \to \infty$ limit (for all Ri) and further find that the optimal global stability limit occurs at $(La_G^{-1}, l_G) = (1.4395, 0.3331)$ for all non-negative Ri at any Pr and for all negative Ri when $Pr = 0$. Of course on noting that thermal effects enter the energy stability counterpart to (2.7*b*) through a term of the form $l^2 Ri(\sigma_2 - 1)\hat{\vartheta}$, we see that this result is synonymous with $\sigma_2 = 1$. For destabilizing (i.e. negative) Ri, however, and $Pr > 0$, we find that $\sigma_2 = -1$, thereby allowing La_G^{-1} to vary with Pr and Ri. Specifically, we find La_G^{-1} diminishes with decreasing Ri, such that $La_G^{-1} \to 0$ as $Ri \to -\infty$. Furthermore the rate at which La_G^{-1} diminishes increases with Pr to the point where $La_G^{-1} = 0$ for all $Ri < 0$ in the limit $Pr \to \infty$.

3.3. *Instability to infinitesimal disturbances*

Turning now to the solution of (2.7) and (2.8) we note that although our neutral stability curves in the $t \to \infty$ limit recover LP's away from onset, they concur near onset only at zero Richardson number, where we find $(La_c^{-1}, l_c) = (1.5157, 0.3187)$ compared with LP's (1.52, 0.32). But, as we see in table 1, our results are vastly different at non-zero Richardson numbers.

Since our numerics accurately reproduced the test cases cited in § 2.2, coding errors seemed unlikely; so we chose to repeat the calculations with LP's basis functions. Our onset values were then within a few percent of LP's. The difference between the two

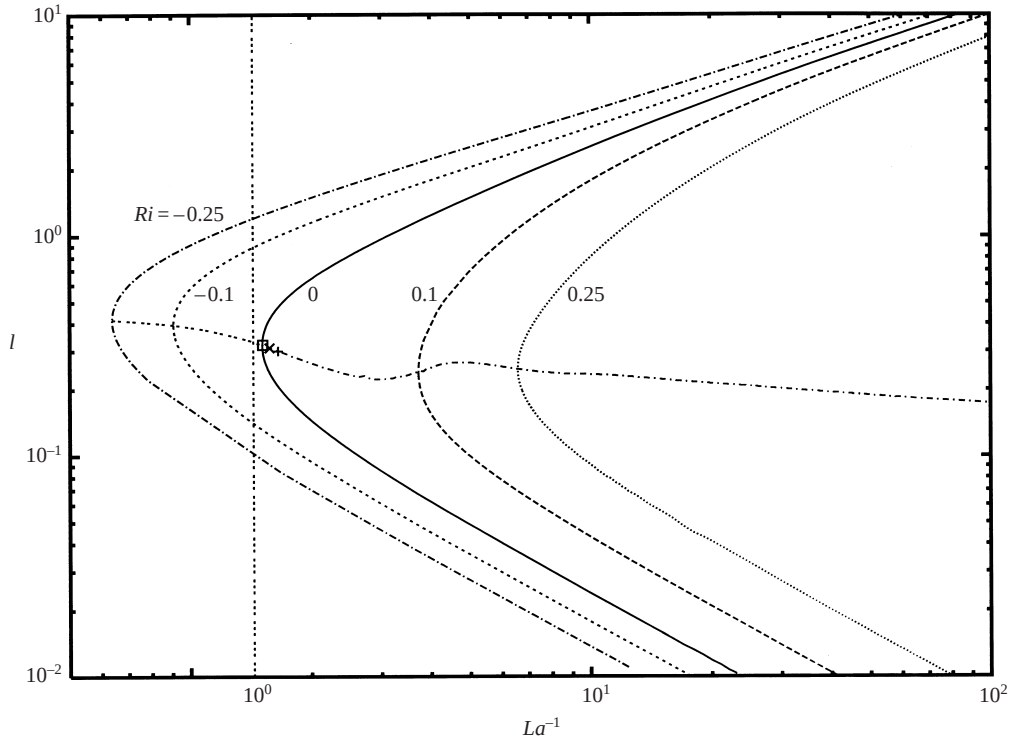

FIGURE 2. Stability diagram showing the optimized global stability estimate for $Ri \geqslant 0$ (vertical line) and lower branch curves of neutral stability for Richardson numbers $Ri = 0, \pm 0.1, \pm 0.25$ at the Prandtl number $Pr = 6.7$. The trace connecting the nose of each curve is that of the critical spacing as Ri increases; see also figures 7 and 8. Symbols denote the onset results of Leibovich & Paolucci (1981): □, $Ri = 0$; ×, $Ri = 0.1$; +, $Ri = 0.25$.

calculations lay with the coefficient matrix $\boldsymbol{A}$, which is well-conditioned near onset with Chebyshev basis functions, but increasingly ill-conditioned as N and Ri increased with LP's functions. In fact we were able to find solutions with LP's functions only for $N \leqslant 10$.

LP's results for $Ri \neq 0$ must thus be discarded. Nevertheless, subcritical instability in the gap $La_G^{-1} < La^{-1} < La_c^{-1}|_{Ri \geqslant 0}$ notwithstanding, LP's conclusion that the $t \to \infty$ neutral curve for $Ri = 0$ is the least stable of their three cases is correct.

Neutral curves for the Ri studied by LP are summarized in table 1. Note that dual values are given for $Ri > 0$: these represent critical values on two branches of the neutral curve, a lower branch which depicts stationary solutions and an upper branch that depicts convective solutions (see also § 4.3), the latter with velocity $u_* a(\sigma/v_T)^{1/2} V_c$. Note also that the convective solutions have two interpretations: the first is that the LCs stand in space and alternate in sign; the second is that a $+V_c$ or $-V_c$ alone each gives rise to spanwise propagating rolls with equal and opposite phase speed.

The lower branch curves are plotted in figure 2. Neutral curves for two negative values of Ri are also plotted in figure 2; these have critical values less than $La_c^{-1}|_{Ri=0}$, in accord with figure 1, but greater than the global values at their respective Richardson numbers.

Our intent now is to explore LP's problem over a wide range of Pr and Ri, considering first stabilizing (§ 4) and then destabilizing (§ 5) Richardson numbers. We

then repeat some calculations (in § 6) using empirical profiles for DU and DD_1, in each instance viewing the results in the light of Smith's (1992) observations in the ocean.

4. The role of Prandtl number with stabilizing Richardson numbers

Although Prandtl number is thought to vary from unity to about ten in the ocean, we vary it from zero to infinity. This allows us to deduce three asymptotes for neutral stability formally, to which our numerics must conform. We begin (§ 4.1) by deducing these asymptotes and then discuss intermediary conditions (§ 4.2); finally (§ 4.3) we look at growth rates at various wavenumbers

4.1. *Limiting cases*

Consider then the inverse Langmuir number at the onset of instability and how it varies with Richardson number in various limiting situations for Pr. First, we can determine formally (from (2.8) and the steady form of (2.7)) that onset at $Pr = 0$ (in the context of $\kappa_T \to \infty$, $\nu_T \neq 0$) is independent of Ri and occurs at some $La_c^{-1} \neq 0$, which must necessarily be the onset value calculated in § 3.3 at $Ri = 0$. Second, by similar means we find that La_c^{-1} becomes independent of Pr as $Ri \to 0$. Thus from table 1 we have that $La_c^{-1}|_{Pr=0} = La_c^{-1}|_{Ri=0} = 1.5157 = La_{c0}^{-1}$, say, which then defines the $Pr = 0$ limit to which all $Pr > 0$ critical curves must asymptote as $Ri \to 0$, as we shall see in figure 3(*b*). It further follows that LP's least stable neutral curve (see § 3.3) is actually the curve defined by the double limit $Ri, Pr \to 0$ and in view of its importance we use it as a reference.

Next, onset in the $Pr \to \infty$ limit (in the context of $\kappa_T \to 0$, $\nu_T \neq 0$), can be interpreted to be either independent of Ri and/or to have the same solution as $Ri = 0$. Thus its asymptote must depict one branch along the $Ri = 0$ axis over some $La^{-1} \geqslant 0$ and, in view of our findings in §3.2, a second branch along the $La^{-1} = 0$ axis for all $Ri < 0$. The possibility also exists for a third branch for $Ri > 0$ at La_{c0}^{-1} (see § 4.3).

Finally, the Miles–Howard theorem (see Drazin & Howard 1966; Leibovich 1983) decrees that inviscid stability is to be expected for $Pr \neq 0$ and $Ri \geqslant 4$ as $La^{-1} \to \infty$, thereby yielding a third asymptote at $Ri = 4$.

Our numerical solutions concur well with these limiting cases, as we shall see in figure 3, although huge inverse Langmuir numbers were necessary to satisfy the inviscid criterion. Curious also is the occurrence of instability at some La^{-1} for $Ri > 4$. In our discussion to follow in § 4.2, therefore, we look first at results for $0 \leqslant Ri < 4$ and then those for $Ri > 4$.

4.2. *Intermediate cases*

We begin by viewing figure 3 where we plot Ri against La_c^{-1}. Observe that La_c^{-1} is single valued in Ri for $0 \leqslant Ri < 4$ at each Pr (= constant > 0) and thus that the flow is unstable to CL2 for all $La^{-1} > La_c^{-1} \geqslant La_{c0}^{-1}$. But of particular interest is how changes in Pr affect instability: interestingly, we see that because La_c^{-1} at constant Ri decreases with decreased Pr, then any decrease in Pr is destabilizing, irrespective of whether Ri and/or La change (increase or decrease), provided $La^{-1} > La_c^{-1} \geqslant La_{c0}^{-1}$ at the final Pr and Ri.

In the ocean context, therefore, where an increase in the turbulence level alters Pr from say its molecular value of 6.7 to nearer unity, we may infer that an increased turbulence level can destabilize a wavy shear flow devoid of LCs to LCs, via the CL2

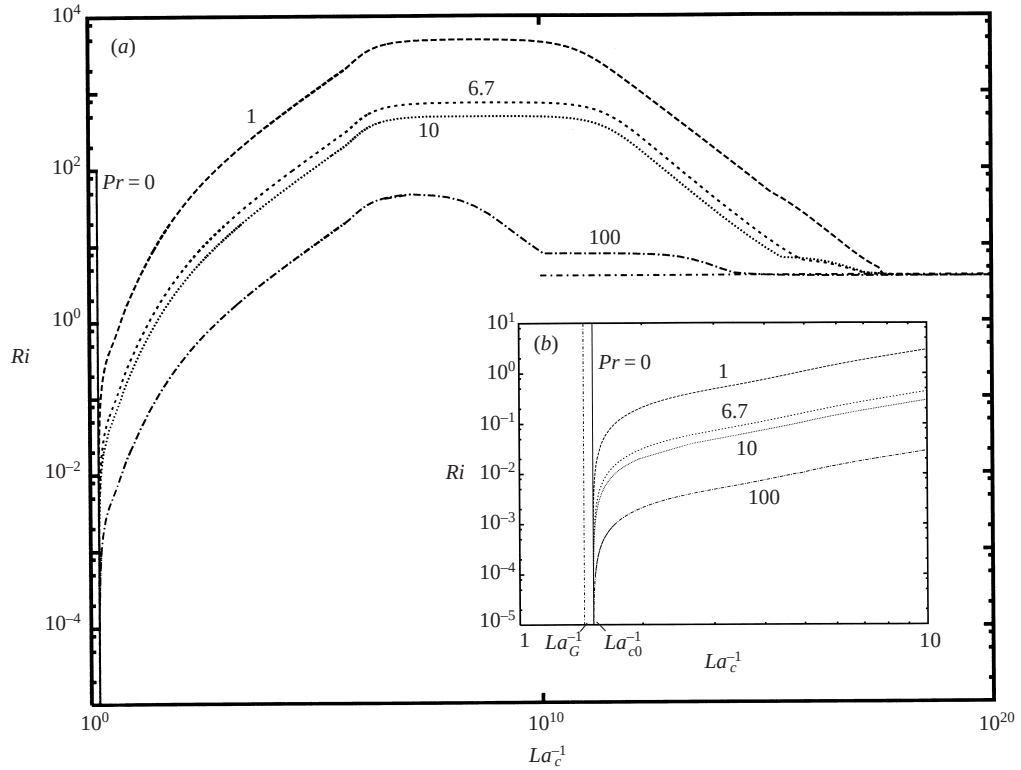

FIGURE 3. Plots of (stabilizing) Richardson number against critical Langmuir number at various Prandtl numbers. Included in (*a*) and (*b*) is the asymptote for $Pr = 0$ at $La_{c0}^{-1} = 1.5157$ and in the expanded view (*b*), the asymptote for global instability, $La_G^{-1} = 1.4402$.

mechanism at constant *La*. This finding resonates with Smith's (1992) observation that, at essentially constant *La*, freshening winds (and consequent increased turbulence level) lead to the formation of LCs (see also §§ 4.3, 4.4) in wind wave conditions theretofor devoid of LCs. Interestingly the changeover occurs in a fifteen minute time frame, which is sufficient time for the intensification of turbulence to depths of circa 5 m (assuming a midrange value of $\nu_T = 0.025\,\mathrm{m^2\,s^{-1}}$ from Huang's (1979) list of ocean eddy viscosities). Of course other factors not envisaged here such as internal waves may also play a role, but the simplicity of the above explanation is compelling.

For $Ri > 4$ on the other hand, La_c^{-1} is multivalued in Ri for constant Pr, but the above conclusion holds, albeit with the caveat that $La_c^{-1} \in [La_{c_{\mathrm{low}}}^{-1}, La_{c_{\mathrm{high}}}^{-1}]$ at the final Pr and Ri. Of course the fact that instability can occur at all for $Ri > 4$ is somewhat unexpected. Indeed, because CL2 is an inviscid instability and inviscidly stable for $Ri > 4$, Leibovich (1980) reasoned it should be stable for all *La*, but in fact the presence of viscosity is mildly destabilizing. 'Mildly' because growth rates for the instability at $Ri = 4$ are from one to four orders of magnitude below their maximal and continue to diminish with increased $Ri > 4$; but they are, nevertheless, positive, as we see in figure 4. This figure, which is typical, is a trace of the maximum growth rate at a constant Langmuir number of $La^{-1} = 10^5$ (at which $l = 0.124$). For ease of comparison, each curve has been normalized to unity at $Ri = 0$, at which point Pr plays no role (see § 4.1); and in fact continues to play no role for $Ri < 2$, as we see in

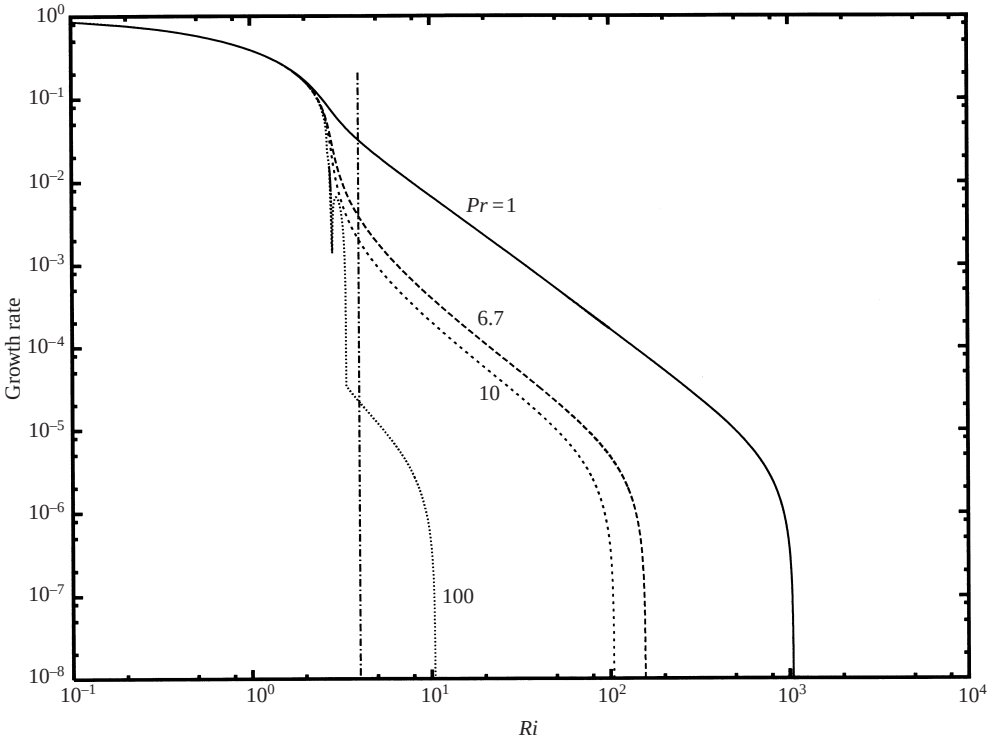

FIGURE 4. Relative growth rates at various Prandtl numbers as a function of Richardson number for $La^{-1} = 10^5$ and $l = 0.124$. The asymptote for inviscid stability is drawn at $Ri = 4$.

figure 4. Of course even though the flow is linearly unstable for $Ri > 4$ this does not guarantee it will be nonlinearly unstable for $Ri > 4$.

4.3. *Neutral stability*

We return now to curves of neutral stability, previously introduced in § 3.3. Here, however, our intent is to explore such curves in detail beginning with the limit cases plotted in figure 5. Included therein is the reference double limit $Pr, Ri \to 0$ solution (LP's least stable curve) from figure 2, which acts as an envelope, and curves representative of the limit $Pr \to \infty$ at $Ri > 0$. In fact for this second limit we plot neutral curves for $Pr = 100$ and $Ri = 1$, and depict not one but two curves specified by the smallest and next smallest onset La^{-1}.

Multiple eigensolutions depicting neutral stability are not of course uncommon in calculations of this type, the curve of smallest La_c^{-1} usually being of interest. But notable here is that the curves depict upper and lower branch eigensolutions, the lower depicting stationary solutions, the upper convective solutions. In the instance plotted the lower branch is nested within the upper; but that is not always the case for, as Pr decreases from infinity, there is a point at which the two branches overlap. Of course in such situations the least stable curve may or may not enclose the nose of the next stable, but whatever the case the onset values of the two curves are usually well separated (see e.g. Phillips 1993, figure 1).

Here, however, the upper and lower branches not only overlap, but there is a Prandtl number, $Pr = Pr_E \approx 8.472$, at which the onset values of the upper and lower branch curves are equal, at $La_c^{-1} = La_{cE}^{-1} \approx 24.85$. This case is also plotted in figure 5.

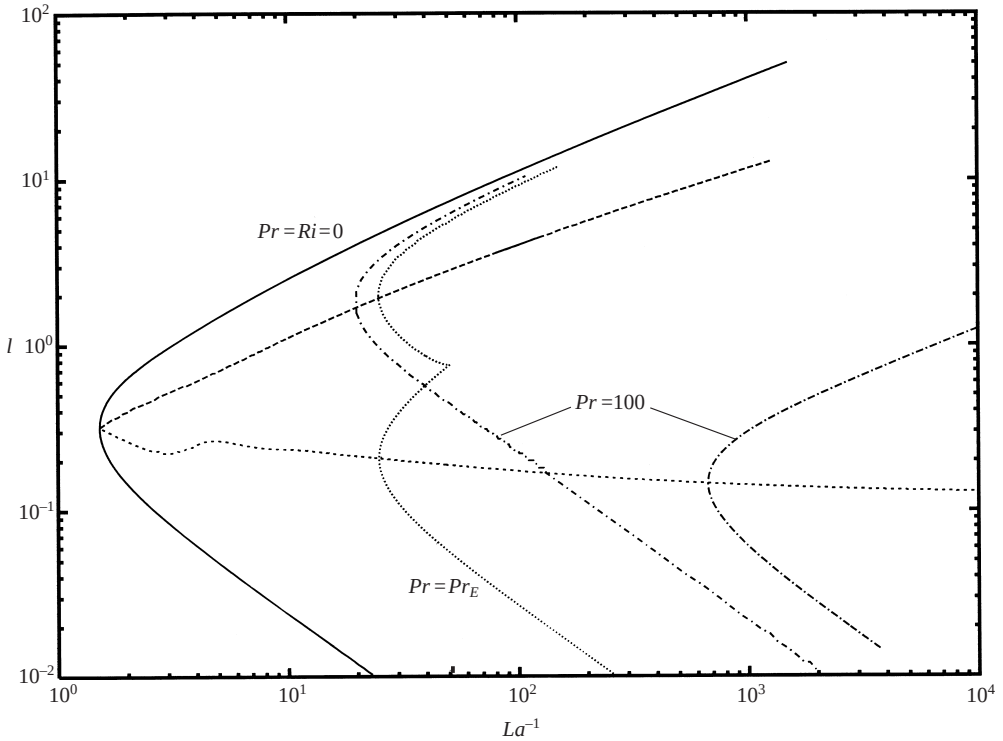

FIGURE 5. Neutral stability curves for various limiting cases. The envelope curve is the double limit $Ri, Pr \to 0$; the other curves are the upper and lower branches of $Ri = 1$, $Pr \to \infty$ and $Pr = Pr_E$. Note that the upper branch curve for $Pr \to \infty$, $Ri = 1$ is essentially coincident with the plotted $Pr = 100$, $Ri = 1$ curve. Noses on the lower branch are connected by the trace of onset spacing. The upper curve is the curve of maximum growth rate for the double limit $Ri, Pr \to 0$. Finally the tick at $La^{-1} = 50$ denotes the location of the growth rate curves drawn in figure 6.

Indeed, as Pr decreases from infinity with $Ri = 1$, we see from figure 5 that La_c^{-1} increases from its value at $Pr \to \infty$ to La_{cE}^{-1} on the upper branch and then decreases from La_{cE}^{-1} to La_{c0}^{-1} on the lower branch. In the process the critical wavenumber l_c at the crossover jumps from about 2.0 to 0.2, so that we would expect the windrow spacing of the LCs to increase from about half the wavelength of the dominant slope waves to roughly five times that wavelength.

4.4. *Growth rates*

Alternatively, if we hold Ri and La^{-1} constant and plot the growth rate as a function of spanwise wavenumber l for various Pr, we obtain curves typified in figure 6. Here $Ri = 1$, $La^{-1} = 50$ and the growth rate is relative to the maximum value for the double limit $Pr, Ri \to 0$ (at the same La^{-1}). Again, as Pr decreases from infinity, the point of maximum growth rate moves from the upper branch to the lower, with a crossover (in this instance) at $Pr \approx 5.3$.

Holding Ri and Pr constant now (with $Pr = 5.3$) and looking at the ensuing neutral curves, we find that La_c^{-1} is smaller on the lower branch but that the growth rate is higher on that branch only until $La^{-1} = 50$. In consequence, as Pr or La^{-1} decrease through $Pr = 5.3$, $La^{-1} = 50$, the windrow spacing increases from about one third the wavelength of the dominant slope waves, to three quarters of that wavelength. Of course this does not mean an abrupt change in spacing occurs at the crossover,

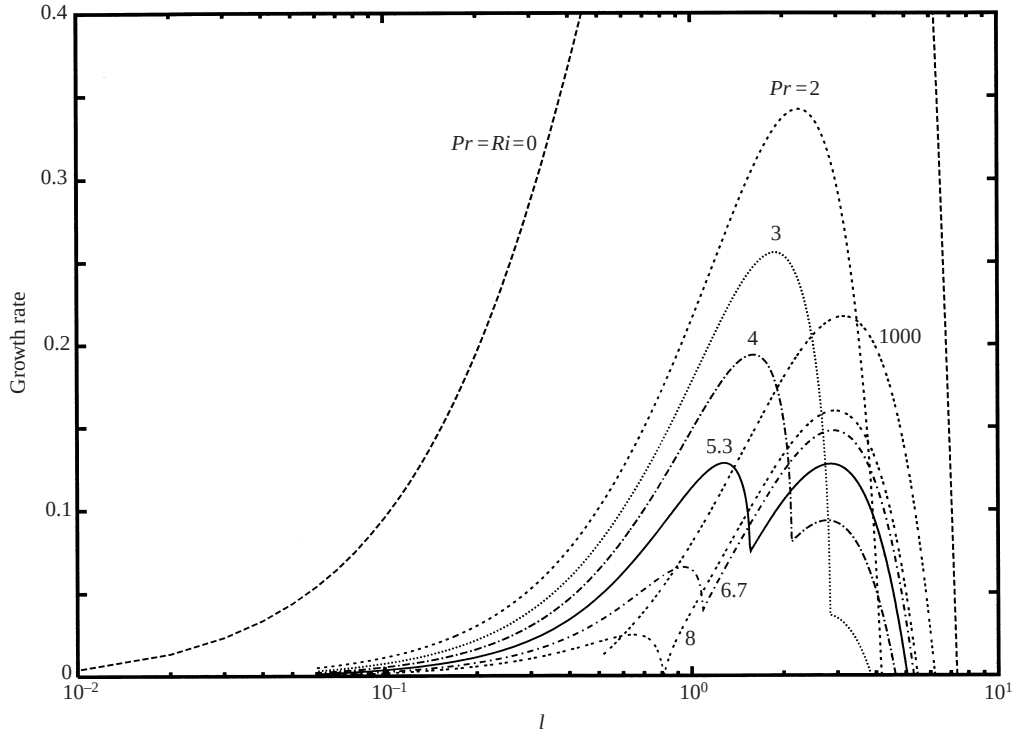

FIGURE 6. Growth rates for various Pr at $La^{-1} = 50$ and $Ri = 1$.

for LCs with both spacings will still form; what it means is that LCs with the larger spacing will persist.

Of course an obvious question at this point is whether the changeover from convective to stationary branches is noticeable in a field experiment? In order to answer this we turn to the windrows described by the LCs and the temporal patterns they depict. While all windrows are basically parallel, LCs which stand in space and alternate in sign (convective see § 3.3) act to form new windrows between the old ones every time they alternate in sign, with dimensionless period $2\pi/(lV_c)$. Convective solutions can also cause a gradual spanwise drift of the windrow field (note that the propagation velocity is less than 10% of the peak transverse velocities in the LCs). Windrows described by stationary LCs on the other hand remain fixed over their lifetime.

In summary, therefore, onset occurs on the upper branch for one range of Pr and Ri and on the lower branch for another range of Pr and Ri. But although crossover is possible at least for $Ri \in (0.03, 1.33)$ and $Pr \in (4.7, 11.5)$, it does not occur for all unstable Pr and Ri.

4.5. *Spanwise wavenumber and curves of maximum growth rate*

We turn now to the spanwise wavenumber and begin with its value at onset, as shown in figure 7. Here we plot l_c as a function of Ri for the lower branch neutral curve. Observe that l_c is a maximum at $Ri = Pr = 0$, which is drawn as an asymptote and that the curves for $Pr > 0$, which peal from that asymptote, take essentially the same form. Indeed, if we plot the same results against La_c^{-1}, we find they collapse, as we see in figure 8. In short, the curve of l_c against La_c^{-1} is independent of Pr.

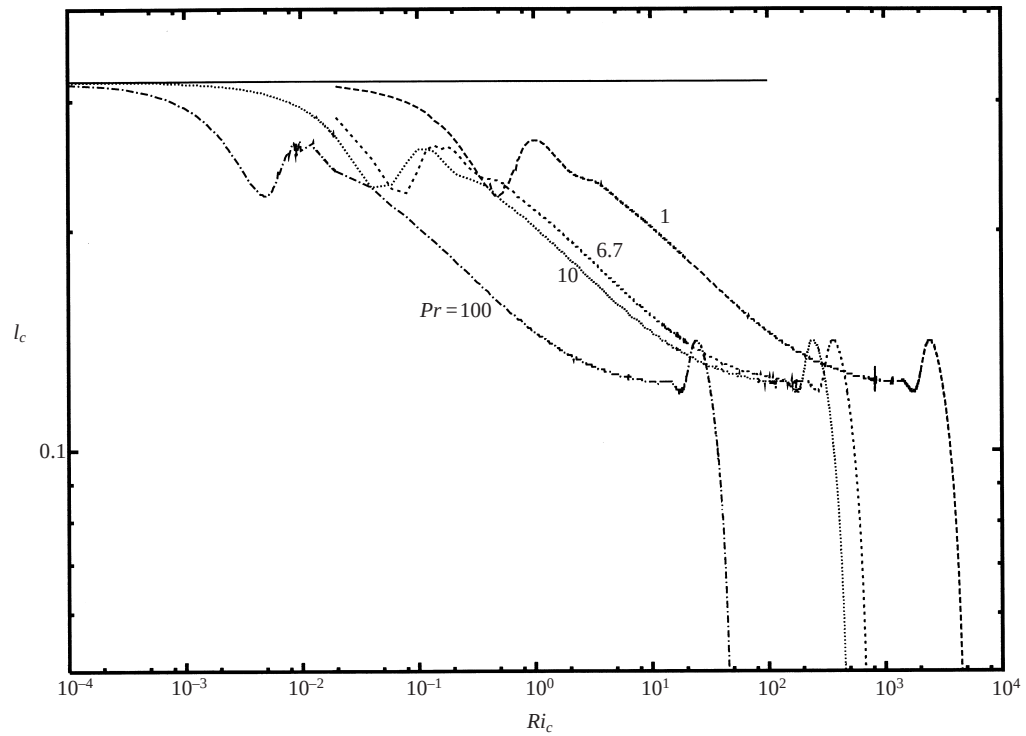

FIGURE 7. Curves of spanwise spacing at onset as a function of Richardson number for various Prandtl numbers.

We do not include the upper branch counterpart of l_c in figures 7 and 8, in part because it extends over only a limited range of Ri and Pr as we discovered in § 4.4, but principally because the ensuing curves are very close, curiously, to the curve of maximum growth rate for the double limit $Pr, Ri \to 0$, as evident in figure 5.

In fact the curve of maximum growth rate for the double limit reference would appear to be something of an asymptote in itself because, different growth rates notwithstanding, the curves of maximum growth rate for both upper and lower branch solutions are asymptotic to it, as we see in figure 9. Note too that, because the dominant spacing is probably specified by the curve of maximum growth rate, we find for fixed Pr and Ri, that the spacing will increase only with diminishing La^{-1}.

5. The role of Prandtl number with destabilizing Richardson number

Although the thermocline in the ocean surface layer is usually neutral or stabilizing, there are occasions when it is destabilizing and we should like now to consider this case. Interestingly, as we found in § 3.2, such conditions no longer limit CL2 to the global lower bound $La_G^{-1}|_{Ri \geqslant 0} = 1.4395$ but permit lower values dependent upon Ri and Pr, as we saw in figure 1.

These same features are also reflected in the critical values depicted in figure 10. In accord with our earlier results, we find that $La_c^{-1} \geqslant La_G^{-1}$ at any combination of Ri and Pr, although here La_c^{-1} seldom exceeds La_G^{-1} by more than one percent and for that reason only La_c^{-1} is shown in 10.

Observe too that $La_c^{-1} \to 0$ for sufficiently large negative Ri, indicating that CL2

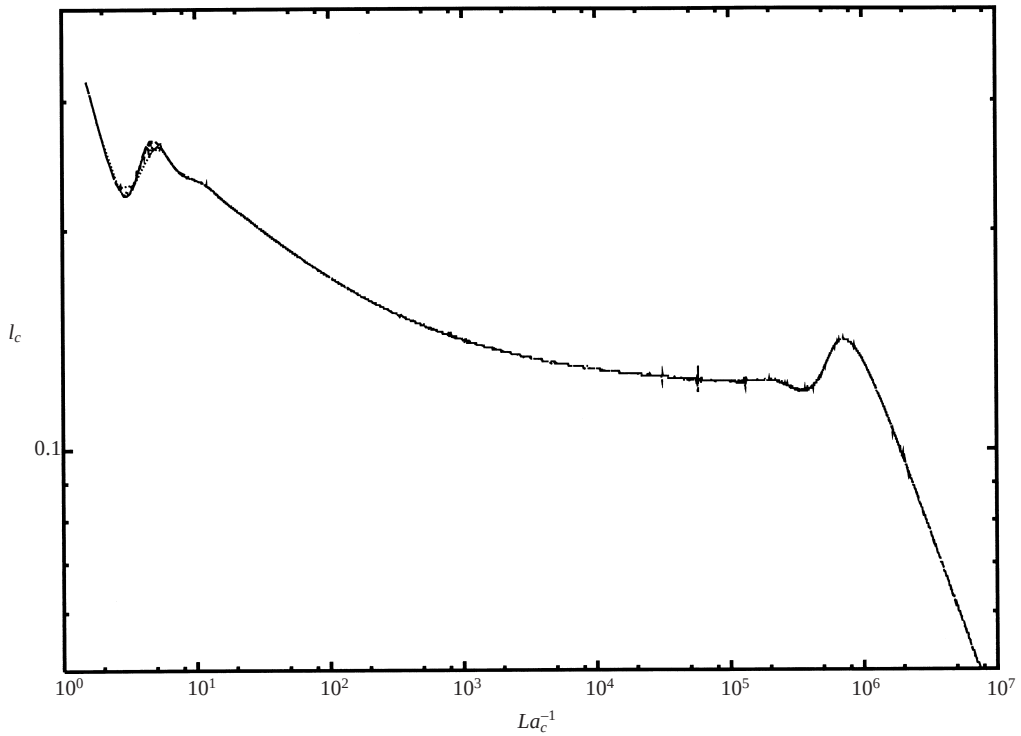

FIGURE 8. Curves of spanwise spacing at onset for various Prandtl and Richardson numbers as shown in figure 7 but plotted as a function of critical Langmuir number.

continues to operate in highly viscous, even creeping flow, situations, provided wave–wave nonlinearities can occur and the wave field is irrotational. Of course rotational waves, which are more the norm in such flows may also excite CL2, but to prove so the calculation must be redone. Specifically (2.3) must be replaced by its rotational counterpart ((4.1) in Phillips 1998) and the Stokes drift must be replaced by the more general wave–wave measure, the pseudomomentum (see Andrews & McIntyre 1978; Phillips 2001*a*). Of course this combination of La_c^{-1} and Ri will doubtless not arise in the ocean, but it may well occur in other contexts.

Neutral stability curves for $Ri < 0$ are drawn in figures 2 and 11. Observe that their generic form is as before but that they now lie to the left or destabilizing side of the reference double limit curve.

6. Results with other primary profiles

While generic profiles for the mean velocity and Stokes drift are useful tools in the study of their instability to LCs, questions always remain regarding the sensitivity of such results to the input primary profiles. Our intent now is to gain insight into this question by employing primary profiles based upon empirical data. Of course like (3.1*a*) or its more general counterparts (Phillips 1996), the velocity field in the ocean is a function of time (see e.g. Plueddemann & Weller 1999). However while the notion of a limiting form as $t \to \infty$ is clear for the theoretical profiles (3.1*a*), the same cannot be said for field experiments (see also § 7). Rather we must accept the data as typical

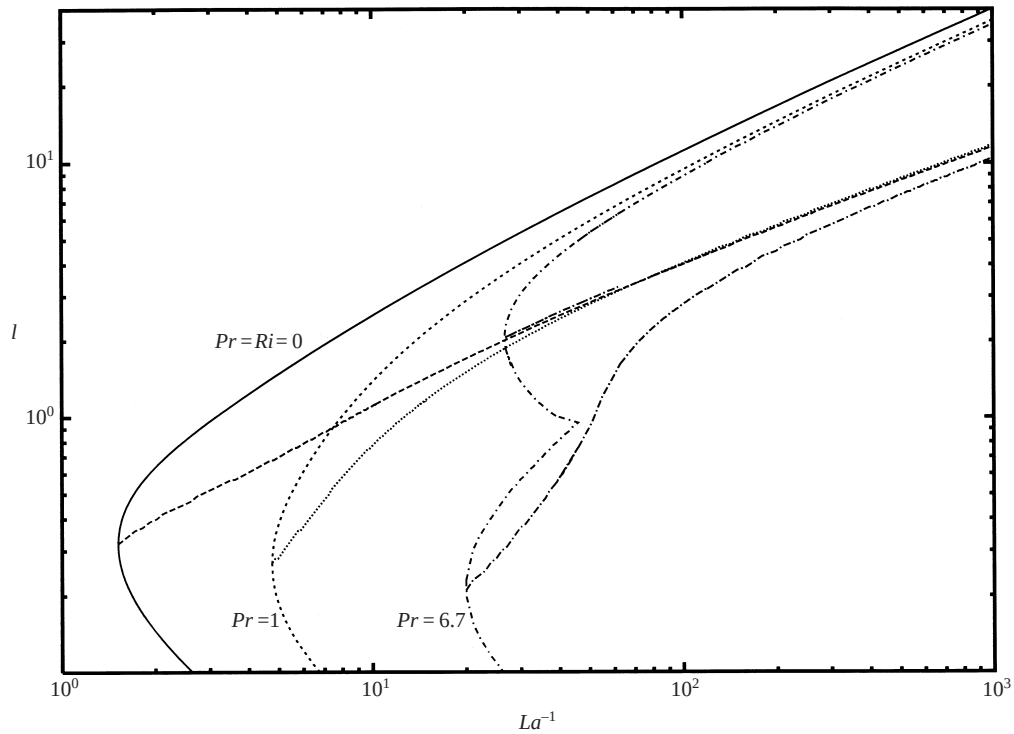

FIGURE 9. Neutral curves and their associated curve of maximum growth rate for various Prandtl numbers at fixed Richardson number $Ri = 1$.

of a mature flow; we must also assume the profile is characteristic of mean events in the absence of LCs.

6.1. *The mean velocity*

Direct measurements of the local mean velocity profile in the ocean surface layer were made as part of the Surface Wave Processes Program (SWAPP) (see e.g. Weller & Plueddemann 1996; Plueddemann *et al.* 1996; Plueddemann & Weller 1999). Of course the profiles are typically three-dimensional so that it is not always clear whether they are in the presence or absence of LCs. Nevertheless, some of Plueddemann & Weller's (1999) data (view their figure 11 with a virtual origin for z) indicate that below one wave amplitude or so the mean shear scales with the law of the wall (for bounded turbulent flows). This finding concurs with the observations of Jones (1985), Richman, deSzocke & Davis (1987) and Lentz (1992). But although law of the wall scaling carries over to the streamwise component of a three-dimensional bounded mean flow (Phillips & Khoo 1987), such scaling is relevant in only some instances in the ocean surface layer, a point Plueddemann & Weller make admirably clear. Nonetheless, a mean velocity field based on such scaling is an appropriate test case and Smith (1992) suggests it be employed.

Here DU is constant at the surface and proportional to z^{-1} some distance from it, in what is known as the logarithmic region. Of course the velocity profile cannot depict logarithmic behaviour indefinitely; there must be an the outer region in which DU approaches zero exponentially fast (Brown & Stewartson 1969). Phillips (1987, 1994) and Phillips & Ratnanather (1990) give expressions that capture such asymptotics

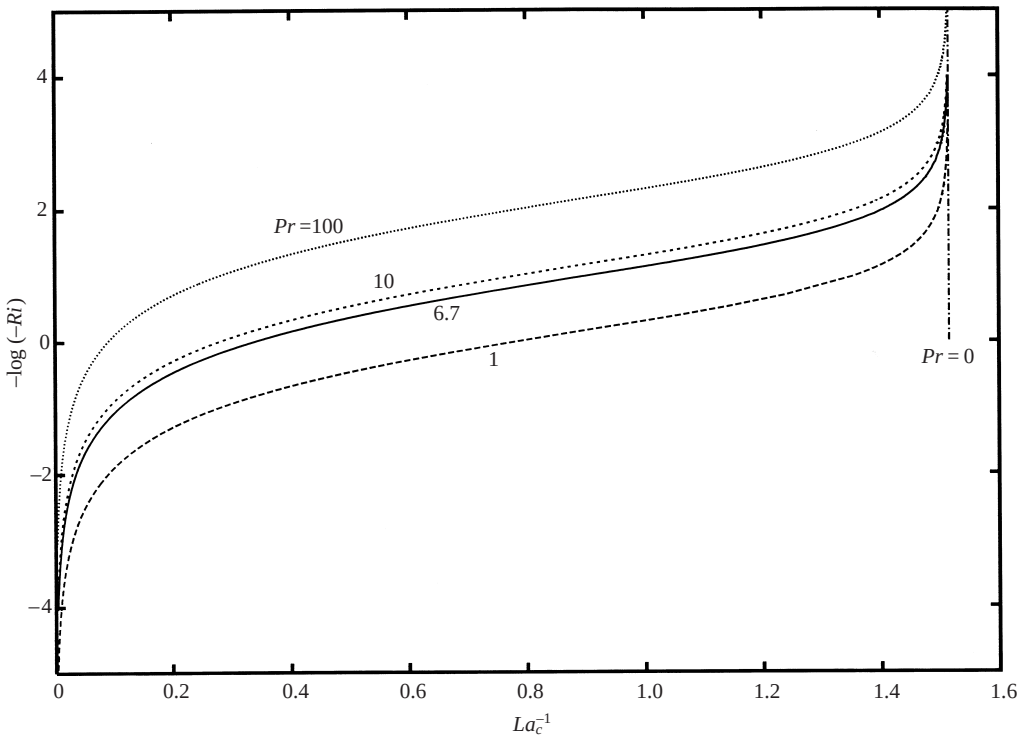

FIGURE 10. Plots of destabilizing (i.e. negative) Richardson numbers against critical Langmuir number for various Prandtl numbers in the $t \to \infty$ limit. Included is the asymptote for $Pr = 0$.

and we employ them here, subject to the assumption that they depict the limiting form of the least stable primary mean velocity profile. Then

$$\mathrm{D}U = \frac{1}{2}\left(\frac{1+\exp-(\kappa\lambda/16)^3}{(1+\frac{1}{8}(\kappa\lambda)^3)^{1/3}}\right) \quad \text{for} \quad 0 \leqslant -z < -z_0, \tag{6.1a}$$

$$= \frac{\exp-(z/z_0-1)^2}{\kappa\lambda} \quad \text{for} \quad -z_0 \leqslant -z < \infty. \tag{6.1b}$$

But to proceed with (6.1) we must relate the independent variable in the vertical direction λ, which is in viscous units, to z. This can of course can be done formally, but the ensuing expression requires knowledge of ν_T/ν, a ratio we prefer to avoid. Instead we employ Jones' finding that $\mathrm{D}U \propto z^{-1}$ for $-z > \alpha a$ and thus associate $z = -\alpha a$ with the edge of the buffer region in a bounded layer, at which point $\lambda \approx 30$. Then because $\alpha a \approx \kappa$ (see Lighthill 1978, p. 454), we have $\kappa\lambda \approx -30z \approx -\mathscr{A}^{1/2}z$.

Of course whether the outer region of the ocean boundary layer has the same structure as its bounded counterpart is decidedly unclear and to our mind unlikely. Nevertheless it is physically necessary that (6.1*b*) apply as $z \to -\infty$ and so we require it from some point z_0, which we arbitrarily set to $z_0 = -2$. The ensuing profile for $\mathrm{D}U$ is plotted in figure 12.

6.2. *The Stokes drift*

Being a Lagrangian measure, the Stokes drift cannot be measured directly by instruments fixed in an Eulerian frame. Nevertheless D_1 can be deduced from measurements

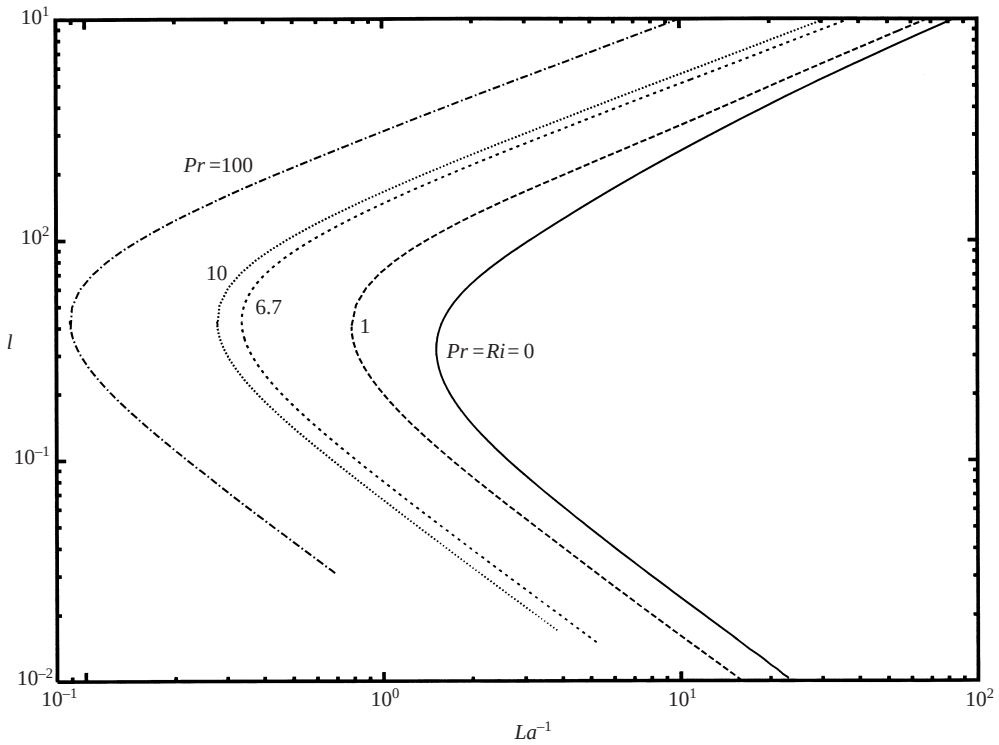

FIGURE 11. Curves of neutral stability for various Pr in the $t \to \infty$ limit with $Ri = -1$.

made by fixed instruments in such a frame, either from knowledge of the spectral density of the wave slope at the free surface (see Huang 1971) or from space–time correlations of velocity fluctuations in the interior (Phillips 2000, 2001*a*). Here we use the former approach and employ Smith's (1992) empirical spectra prior to and after the formation of LCs.

In fact Smith gives an expression for D_1, but in deriving it he approximates the spectral density (of wave slope) by two regions of the form $B_i\sigma^{n_i}$, with $n_i = [0, 0]$. Our reading is that the curve is better approximated by three regions in which $n_i = [0, 3, 0]$. For irrotational surface waves in deep water we then find that

$$\begin{aligned} \mathrm{D}D_1 = \mathscr{C}_1 \{ \xi^{-1} [B_1(\mathrm{erf}(S_2\xi) - \mathrm{erf}(S_1\xi)) + B_3(\mathrm{erf}(S_c\xi) - \mathrm{erf}(S_3\xi))] \\ -\mathscr{C}_2 B_2 \xi^{-2} \left[S_3^2 \exp -(S_3\xi)^2 - S_2^2 \exp -(S_2\xi)^2 + \xi^{-2}(\exp -(S_3\xi)^2 - \exp -(S_2\xi)^2) \right] \}, \end{aligned} \tag{6.2}$$

which of course recovers Smith's expression if $S_3 = S_2$. Here $\xi = (-2z)^{1/2}$, $\mathscr{C}_1 = b(3\pi/2)^{1/2}\kappa^{-2}$, $\mathscr{C}_2 = (g/2\pi f_0 W)^3/\sqrt{\pi}$ and $S_i = 2\pi W f_i/g$. Finally we note that

$$\mathrm{D}D_1 \sim \frac{2\mathscr{C}_1}{\sqrt{\pi}} [B_1(S_2 - S_1) + B_3(S_c - S_3)] \quad \text{as} \quad z \to 0 \tag{6.3}$$

from which we determine the constant b to ensure $\mathrm{D}D_1(0) = 4$, as is the case in §§ 3 and 4.

Smith's data (his figure 13) suggest that $f_i = [0.088, 0.138, 0.26]$ Hz with $B_i = [0.3, 113.8, 2.0] \times 10^{-3}$ prior to the formation of LCs (when the wind speed $W = 8\,\mathrm{m\,s^{-1}}$) and $f_i = [0.088, 0.12, 0.26]$ Hz with $B_i = [0.45, 256.0, 4.5] \times 10^{-3}$ after LCs

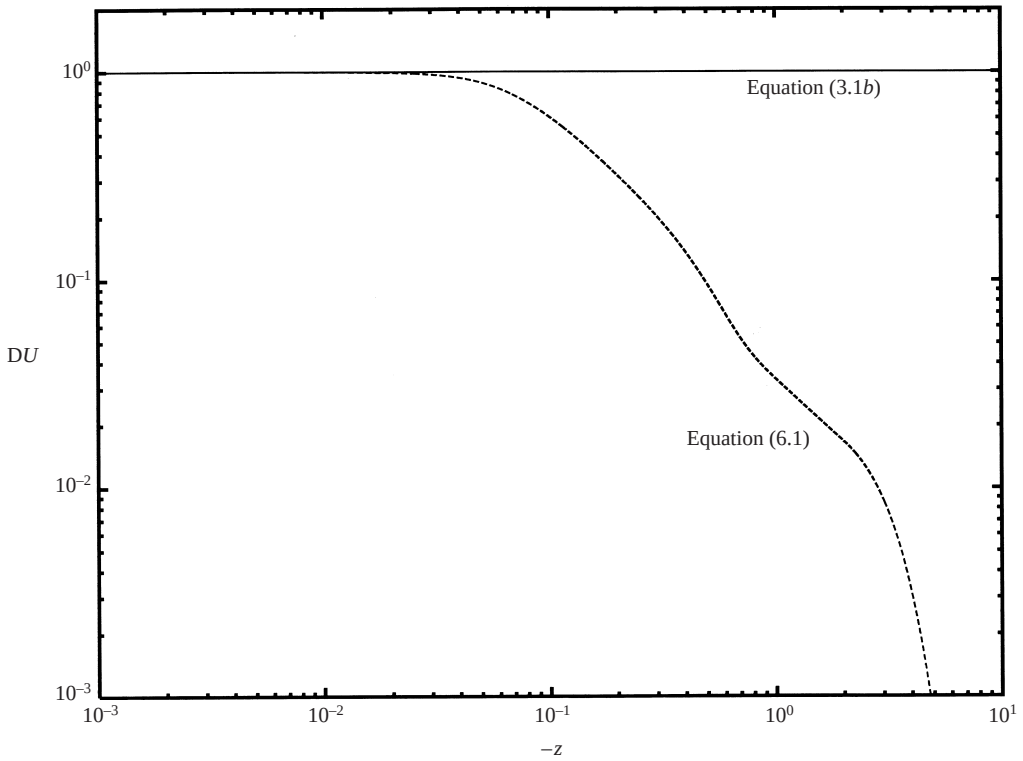

FIGURE 12. Gradients of mean velocity for accelerating laminar flow as $t \to \infty$ (see (3.1*b*)) and fully developed turbulent flow (6.1).

form, when $W = 13\,\mathrm{m\,s^{-1}}$. Finally for convenience we set the reference frequency $f_0 = 1\,\mathrm{Hz}$ and, because the data end at $f = 0.65\,\mathrm{Hz}$, take that value as the cut-off frequency f_c.

Before and after traces of $\mathrm{D}D_1$ are plotted in figure 13 along with its monochromatic counterpart. Observe that $\mathrm{D}D_1$ for the measured spectra diminishes more rapidly with depth than $4\mathrm{e}^{2z}$, at least for $-z < 3$.

6.3. *Results*

Our first task is to deduce the influence $\mathrm{D}U$ has on stability and thus calculate neutral stability curves for both velocity gradients, i.e. (3.1*b*) and (6.1), in the presence of the same Stokes drift gradient, that for monochromatic waves (3.2). As evident in figure 14, relative to the mean laminar profile, the mean turbulent profile acts to stabilize the interaction, altering onset from $La_c^{-1} = La_{c0}^{-1}$ to $La_c^{-1} = 8.912$. This result is perhaps not surprising because we earlier determined that the least stable scenario occurs when the full extent of the LCs is subjected to uniform shear, which is the case for (3.1*a*) when $t \to \infty$, but not the case for (6.1).

To determine the influence of Stokes drift then, we retain the least stable velocity gradient and repeat the calculation. Here we find that a spectrum of waves, as opposed to monochromatic waves, is also stabilizing, but that the degree to which they stabilize is very much dependent upon details of the spectrum. Indeed we find onset occurs at $La_c^{-1} = 2.97$ for the spectrum prior to Smith's observation of LCs and $La_c^{-1} = 7.2$ after. Of course the same holds true if we employ the turbulent velocity profile, only

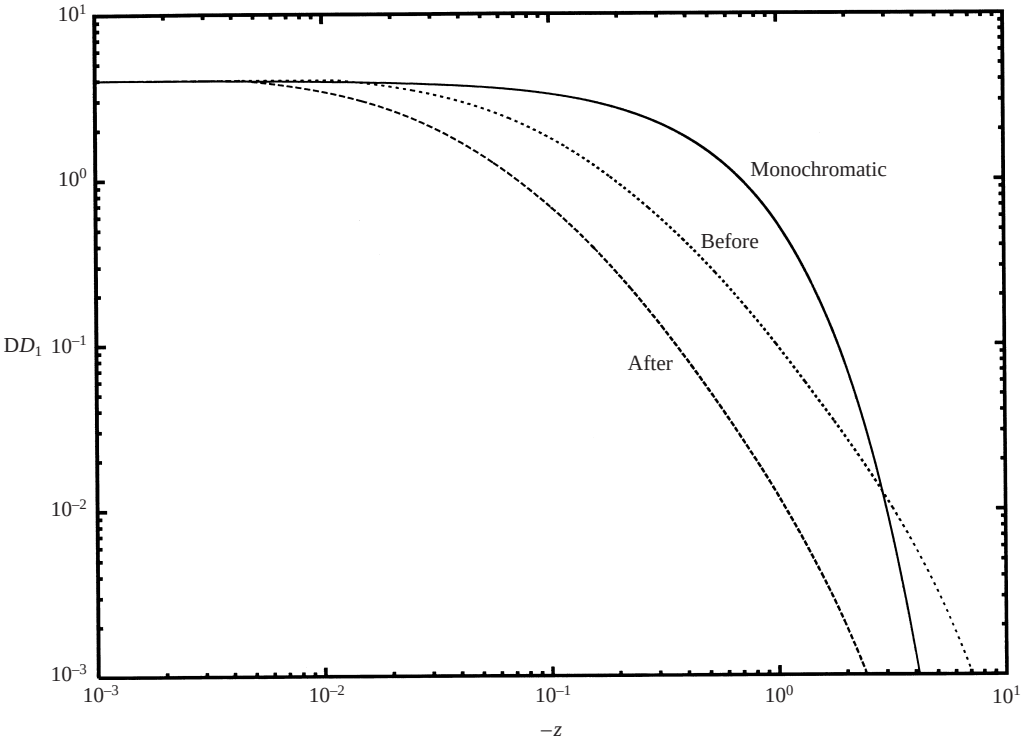

FIGURE 13. Gradients of Stokes drift for monochromatic two-dimensional waves and developing seas before and after the formation of Langmuir cells.

now onset is delayed until $La_c^{-1} = 16.88$ (before) and $La_c^{-1} = 38.72$ (after), as we see in figure 14. In conclusion, therefore, although $La_c^{-1} = La_{c0}^{-1}$ may well be the critical value for instability to LCs in all situations for which $Ri \geqslant 0$, the actual onset La^{-1} is non-unique and strongly dependent upon Ri, Pr and details of the shear and wave spectrum that apply locally.

Finally, rather than enforcing the boundary condition $DD_1(0) = 4$, we allow $DD_1(0)$ to take its measured value by setting $b = 1$ in (6.2); physically this adjusts the intensity level of the Stokes drift to that present in the ocean. Then with the mean shear (6.1), onset values range from $La_c^{-1} = 131$ with $Ri = 0$, to $La_c^{-1} = 6292$ with $Ri = 0.1$ and $Pr = 6.7$. These values vastly exceed those above, but they are precisely in the range $La^{-1} = 10^2$–10^3 which Leibovich (1977*b*) argues are of interest in the ocean.

7. Discussion

Two questions come to mind regarding CL2: the first is physical and asks whether CL2 is the mechanism primarily responsible for LCs in the ocean; the second is pragmatic and asks, irrespective of question one, whether CL2 can credibly depict the more important features of the lifecycle of LCs, as required in the next generation of Global change models. The present work cannot answer the first question but it does shed light on the second.

In particular we now have an explanation for two of Smith's observations: his first was the absence and presence of LCs at essentially the same Langmuir number. This (see § 4.2) can be explained by diminishing values of Pr, which occur owing to an

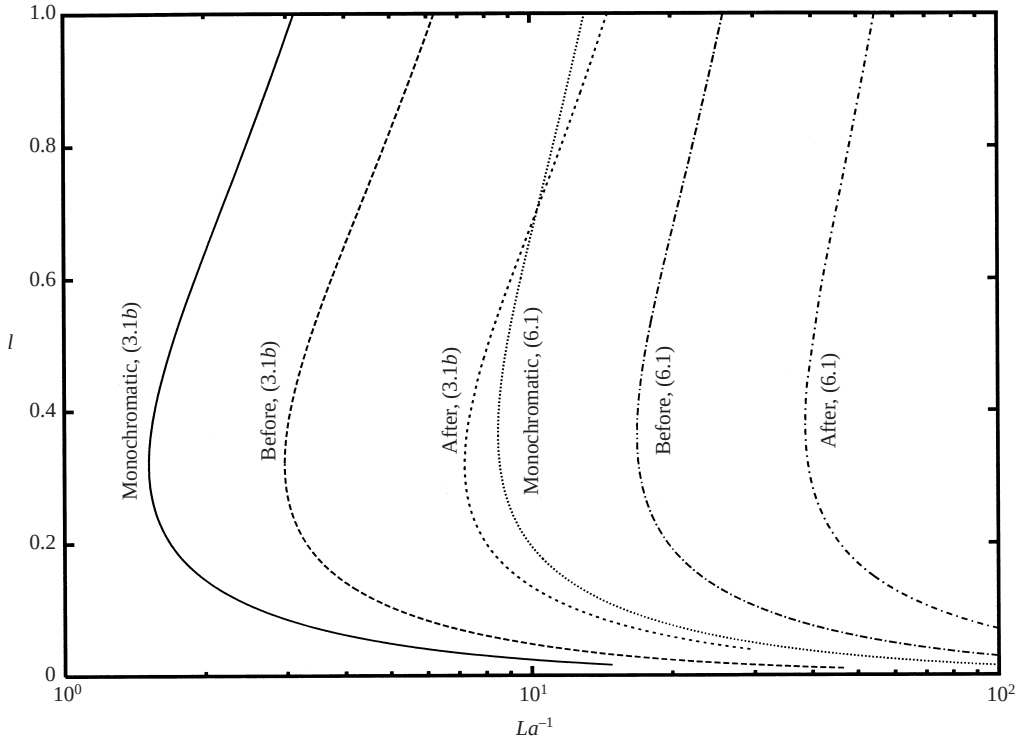

FIGURE 14. Curves of neutral stability at $Ri = 0$ for various mean velocity and Stokes drift profiles.

increased level of turbulence brought on by freshening winds. In essence diminishing values of Pr are destabilizing to LCs at constant La^{-1}, provided $Ri \neq 0$.

Smith's second observation concerned the spacing of the LCs, which increases with time. When first observed these were less (11–16 m) than the 25 m dominant wavelength of the waves but grew in time to well exceed that wavelength. Since the resolution of Smiths data is limited to about 10 m, we do not know if LCs were present prior to Smith being aware of them. But irrespective of when LCs first formed, we need an explanation for windrow spacings less than the dominant wavelength of the waves and that requires $l > 1$. If La^{-1} is constant and Pr decreasing as above, we can achieve $l > 1$ via the present analysis only if the neutral curve has an upper branch, because the lower branch requires $l < 1$. Fortuitously upper and lower branch neutral curves do exist and, as we found in § 4.3, crossover from one to the other can occur for some Pr and Ri, namely $Pr \in (4.7, 11.5)$ and $Ri \in (0.03, 1.33)$, so we can satisfy $l > 1$. Furthermore as Pr falls, it must at some point exit the range 4.7–11.5, thereby forcing crossover to the lower branch, from which point LCs with larger spacings will dominate. Of course this scenario does not exclude dynamical effects which may increase spacing via nonlinearities that occur once LCs have formed; nor does it exclude a cascade in scales by which LCs form, as we shall now discuss.

A curious result of this analysis is the least stable scenario which, as LP determined, occurs in the limit $t \to \infty$. Physically (see (3.1*b*)) this means that the full extent of the LCs are subjected to uniform shear and this raises an interesting question: if LCs originate because of the dominant waves as the analysis in § 2.1 assumes, then it is doubtful whether LCs ever arise in the least stable limit because the uniform region of the shear layer is just not that deep. Alternatively if LCs do arise in the least

stable limit, then the wavelength of the waves exciting them is much smaller than the wavelength of the dominant waves, and rather than weak shear as the base flow, for which $s = 2$ (see § 2.1), we have strong shear $s = 0$. Interestingly the latter is the case in Melville *et al.*'s (1998) laboratory experiments, which highlight the rapid growth of LCs, although whether CL2 is the instability mechanism that spawns them is unclear. Of course CL2 does carry over to $s = 0$ shear (Craik 1982) but the character of the instability is vastly different (Craik 1982; Phillips & Wu 1994; Phillips 1998) from the $s = 2$ case studied here. Nevertheless, such findings in combination with Smith's observation (of no LCs in steady wind wave conditions followed by LCs of increasing spacing in freshening conditions; see § 1) fuel the notion (Phillips, Wu & Jahnke 1999) that ocean LCs originate in the strong shear ($s = 0$) regime and then grow in scale as they cascade through medium ($s = 1$) to ultimately weak ($s = 2$) shear, only to be sustained by the dominant waves.

This work was supported by the National Science Foundation through OCE grants 9696161 and 9818092.

REFERENCES

Andrews, D. G. & McIntyre, M. E. 1978 An exact theory of nonlinear waves on a Lagrangian-mean flow. *J. Fluid Mech.* **89**, 609–646.

Baines, P. G. & Gill, A. E. 1969 On Thermohaline convection with linear gradients. *J. Fluid Mech.* **37**, 289–306.

Brown, S. N. & Stewartson, K. 1969 Laminar separation. *Ann. Rev. Fluid Mech.* **1**, 45–72.

Cox, S. M. & Leibovich, S. 1993 Langmuir circulations in a surface layer bounded by a strong thermocline. *J. Phys. Oceanogr.* **23**, 1330–1345.

Cox, S. M. & Leibovich, S. 1997 Large-scale three-dimensional Langmuir circulation. *Phys. Fluids* **9**, 2851–2863.

Cox, S. M., Leibovich, S., Moroz, I. M. & Tandon, A. 1992 Non-linear dynamics in Langmuir circulations with $O(2)$ symmetry. *J. Fluid Mech.* **241**, 669–704.

Craik, A. D. D. 1970 A wave-interaction model for the generation of windrows. *J. Fluid Mech.* **41**, 801–821.

Craik, A. D. D. 1977 The generation of Langmuir circulations by an instability mechanism. *J. Fluid Mech.* **81**, 209–223.

Craik, A. D. D. 1982 Wave-induced longitudinal-vortex instability in shear layers. *J. Fluid Mech.* **125**, 37–52.

Craik, A. D. D. & Leibovich, S. 1976 A rational model for Langmuir circulations. *J. Fluid Mech.* **73**, 401–426.

Drazin, P. G. & Howard, L. N. 1966 Hydrodynamic instability of parallel flow in inviscid fluid. In *Advances in Applied Mechanics*, vol. 7 (ed. G. Kuerti), pp 1–89. Academic Press.

Drazin, P. G. & Reid, W. H. 1981 *Hydrodynamic Stability*. Cambridge University Press.

Gargett, A. E. 1989 Ocean turbulence. *Ann. Rev. Fluid Mech.* **21**, 419–451.

Huang, N. E. 1971 Derivation of Stokes drift for a deep-water random gravity wave field. *Deep-Sea Res.* **18**, 255–259.

Huang, N. E. 1979 On surface drift currents in the ocean. *J. Fluid Mech.* **91**, 191–208.

Jones, I. 1985 Turbulence below wind waves. In *The Ocean Surface* (ed. Y. Toba & H. Mitsuyasu), pp. 437–442. D. Reidel.

Kenney, B. C. 1993 Observations of coherent bands of algae in a surface shear layer. *Limnol. Oceanogr.* **38**, 1059–1067.

Langmuir, I. 1938 Surface motion of water induced by wind. *Science* **87**, 119–123.

Leibovich, S. 1977*a* Convective instability of stably stratified water in the ocean. *J. Fluid Mech.* **82**, 561–585.

Leibovich, S. 1977*b* On the evolution of the system of wind drift currents and Langmuir circulations in the ocean. Part 1. Theory and averaged current. *J. Fluid Mech.* **79**, 715–743.

Leibovich, S. 1980 On wave-current interaction theories of Langmuir circulations. *J. Fluid Mech.* **99**, 715–724.

Leibovich, S. 1983 The form and dynamics of Langmuir circulations. *Ann. Rev. Fluid Mech.* **15**, 391–427.

Leibovich, S., Lele, S. & Moroz, I. M. 1989 Nonlinear dynamics in Langmuir circulations and thermosolutal convection. *J. Fluid Mech.* **198**, 471–511.

Leibovich, S. & Paolucci, S. 1980 Energy stability of the Eulerian-mean motion in the upper ocean to three-dimensional perturbations. *Phys. Fluids* **23**, 1286–1290.

Leibovich, S. & Paolucci, S. 1981 The instability of the ocean to Langmuir circulations. *J. Fluid Mech.* **102**, 141–167.

Leibovich, S. & Ulrich, D. 1972 A note on the growth of small scale Langmuir circulations. *J. Geophys. Res.* **77**, 1683–1688.

Lentz, S. J. 1992 The surface boundary layer in coastal upwelling regions. *J. Phys. Oceanogr.* **22**, 1518–1539.

Li, M. & Garrett, C. 1993 Cell merging and the jet/downwelling ratio in Langmuir circulation. *J. Mar. Res.* **51**, 737–769.

Li, M. & Garrett, C. 1997 Mixed layer deepening due to Langmuir circulation. *J. Phys. Oceanogr.* **27**, 121–132.

Li, M., Zahariev, K. & Garrett, C. 1995 Role of Langmuir circulation in the deepening of the ocean surface mixed layer. *Science* **270**, 1955–1957.

Lighthill, M. J. 1978 *Waves in Fluids.* Cambridge University Press.

McWilliams, J. C., Sullivan, P. P. & Moeng, C.-H. 1997 Langmuir circulations in the ocean. *J. Fluid Mech.* **334**, 1–30.

Melville, W. K., Shear, R. & Veron, F. 1998 Laboratory measurements of the generation and evolution of Langmuir circulations. *J. Fluid Mech.* **364**, 31–58.

Phillips, W. R. C. 1987 The wall region of a turbulent boundary layer. *Phys. Fluids* **30**, 2354–2362.

Phillips, W. R. C. 1993 The genesis of longitudinal vortices in free and bounded shear layers. In *Eddy Structure Identification in Free Turbulent Shear Flows* (ed. J. Bonnet & M. Glauser), pp. 35–41. Kluwer.

Phillips, W. R. C. 1994 On the logarithmic law constants and the turbulent boundary layer at low Reynolds numbers. *Appl. Sci. Res.* **52**, 279–293.

Phillips, W. R. C. 1996 On a class of unsteady boundary layers of finite extent *J. Fluid Mech.* **319**, 151–170.

Phillips, W. R. C. 1998 Finite amplitude rotational waves in viscous shear flows. *Stud. Appl. Maths* **101**, 23–47.

Phillips, W. R. C. 2000 Eulerian space-time correlations in turbulent shear flows. *Phys. Fluids* **12**, 2056–2064.

Phillips, W. R. C. 2001*a* On the pseudomomentum and generalized Stokes drift in a spectrum of rotational waves. *J. Fluid Mech.* **430**, 209–229.

Phillips, W. R. C. 2001*b* Langmuir circulations beneath growing or decaying surface waves. *J. Fluid Mech.* (submitted).

Phillips, W. R. C. & Khoo, B. C. 1987 The vortex boundary layer beneath a Rankine-like vortex. *Proc. R. Soc. Lond.* A **411**, 177–192.

Phillips, W. R. C. & Ratnanather, T. 1990 The outer region of a turbulent boundary layer. *Phys. Fluids* A **2**, 427–434.

Phillips, W. R. C. & Wu. Z. 1994 On the instability of wave-catalysed longitudinal vortices in strong shear. *J. Fluid Mech.* **272**, 235–254.

Phillips, W. R. C., Wu, Z. & Jahnke, C. C. 1999 Longitudinal vortices in wavy boundary layers. In *Wind-Over-Wave Couplings: Perspectives and Prospects* (ed. S. G. Sajjadi, N. H. Thomas & J. C. R. Hunt), pp. 41–47. Oxford University Press.

Phillips, W. R. C., Wu. Z. & Lumley, J. L. 1996 On the formation of longitudinal vortices in turbulent boundary layers over wavy terrain. *J. Fluid Mech.* **326**, 321–341.

Plueddemann, A. J., Smith, J. A., Farmer, D. M., Weller, R. A., Crawford, W. R., Pinkel, R., Vagle, S. & Gnanadesikan, A. 1996 Structure and variability of Langmuir circulation during the Surface Waves Processes Program. *J. Geophys. Res.* **101**, 3525–3543.

Plueddemann, A. J. & Weller, R. A. 1999 Structure and evolution of the oceanic surface boundary layer during the Surface WAves Processes Program. *J. Mar. Syst.* **21**, 85–102.

Richman, J. G., deSzocke, R. A. & Davis, R. E. 1987 Measurements of near surface shear in the ocean. *J. Geophys. Res.* **92**, 2851–2858.

Skyllingstad, E. D. & Denbo, D. W. 1995 An ocean large eddy simulation of Langmuir cells and convection in the surface mixed layer. *J. Geophys. Res.* **100**, 8501–8522.

Smith, J. A. 1992 Observed growth of Langmuir circulation. *J. Geophys. Res.* **97**, 5651–5664.

Smith, J. A. 1998 Evolution of Langmuir circulation in a storm. *J. Geophys. Res.* **103**, 12649–12668.

Smith, J., Pinkel, R. & Weller, R. A. 1987 Velocity structure in the mixed layer during MILDEX. *J. Phys. Oceanogr*, **17**, 425–439.

Spalart, P. R., Moser R. D. & Rogers M. M. 1991 Spectral methods for the Navier–Stokes equations with one infinite and two periodic directions. *J. Comput. Phys*, **96**, 297–324.

Thorpe, S. A. & Hall, A. J. 1982 Observations of the thermal structure of Langmuir circulation. *J. Fluid Mech.* **114**, 237–250.

Weller, R. A., Dean, J. P., Marra, J., Price, J. F., Francis, E. A. & Broadman, D. C. 1985 Three-dimensional flow in the upper ocean. *Science* **227**, 1552–1556.

Weller, R. A. & Plueddemann, A. J. 1996 Observations of the vertical structure of the oceanic boundary layer. *J. Geophys. Res.* **101**, 3525–3543.

Weller, R. A. & Price, J. F. 1988 Langmuir circulation within the oceanic mixed layer. *Deep-Sea Res.* **35**, 711–747.

Zedel, L. & Farmer, D. 1991 Organized structures in subsurface bubble clouds: Langmuir circulation in the upper ocean. *J. Geophys. Res.* **96**, 8889–8900.